Climate and Vegetation: An ERA-Interim and GIMMS NDVI Analysis

DANLU CAI,* KLAUS FRAEDRICH,+ FRANK SIELMANN,# YANNING GUAN,+ SHAN GUO,+ LING ZHANG,@ AND XIUHUA ZHU#

* *Institute of Remote Sensing and Digital Earth, Chinese Academy of Sciences, Beijing, China, and Max Planck Institute for Meteorology, Hamburg, Germany, and University of the Chinese Academy of Sciences, Beijing, China*
+ *Institute of Remote Sensing and Digital Earth, Chinese Academy of Sciences, Beijing, China*
# *KlimaCampus, University of Hamburg, Hamburg, Germany*
@ *Max Planck Institute for Meteorology, Hamburg, Germany*

(Manuscript received 29 October 2013, in final form 8 January 2014)

ABSTRACT

To complement geographical presentation of remote sensing vegetation information, the authors apply Budyko's physical state space diagram to analyze functional climate relations. As an example, the authors use Interim ECMWF Re-Analysis (ERA-Interim) global weather data to provide the statistics (1982–2006) of climate states in a two-dimensional state space spanned by water demand (net radiation N) versus water/energy limitation (dryness ratio D of net radiation over precipitation). Embedding remote sensing–based Global Inventory Modeling and Mapping Studies (GIMMS) data [normalized difference vegetation index (NDVI) > 0.1] shows the following results: (i) A bimodal frequency distribution of unit areas (pixels) is aligned near $D \sim 1$ but separated meridionally, associated with higher and lower net radiation. (ii) Vegetation states are represented as (N, D, NDVI) triplets that reveal temperate and tropical forests crossing the border ($D \sim 1$) separating energy- and water-limited climates but unexpectedly show that they also exist in marginal regions (few pixels) of large dryness. (iii) Interannual variability of dryness is lowest where the largest climate mean NDVI values of greenness (forests) occur. The authors conclude that the combined (N, D, NDVI) analysis based on climate means has shown that tropical and temperate forests (NDVI > 0.6) are (i) not restricted to the energy-limited domain $D < 1$ (extending into the water-limited surface climate regime) and (ii) associated with low interannual variability of dryness. Thus, measures of interannual variability may be included in Budyko's classical framework of geobotanic analysis of surface climates.

1. Introduction

Vegetation coverage and vegetation type are mainly controlled by both water supply and demand, which are measured in terms of climate variables taken as long-term means of weather information. A first step relating vegetation and climate was introduced by Köppen (1936) delineating vegetation-based climate types to two controlling factors, rainfall and temperature averages. Quantitative measures of global distributions of vegetation coverage, vegetation type, and vegetation change are available from satellite-based datasets and analyses, which have the advantage that they are spatially extensive and temporally frequent. That is, the global vegetation state is monitored by the satellite-based normalized difference vegetation index (NDVI), which is closely related to percent green cover. The Global Inventory Modeling and Mapping Studies (GIMMS) NDVI data have been observed for about 25 yr (late 1981–2006; Tucker et al. 2004), thus covering a climate-relevant time scale. Furthermore, NDVI is linked to the fraction of photosynthetically active radiation (fPAR) absorbed by vegetation and therefore to gross primary productivity as demonstrated by satellite-based analyses of land surface vegetation (Asrar et al. 1984; Carlson and Ripley 1997; Myneni et al. 1995).

Thus, satellite-based vegetation types by NDVI combined with the Interim European Center of Medium-Range Weather Forecasts (ECMWF) Re-Analysis (ERA-Interim) provide suitable datasets for a combined vegetation and climate analysis. Here, they are subjected to Budyko's framework (Budyko 1956, 1974; Budyko et al. 1986), which has inspired physical insights on the control of the rainfall–runoff chain in terms of

Corresponding author address: Danlu Cai, Max Planck Institute for Meteorology, Bundesstrasse 53, Hamburg, 20146 Germany.
E-mail: danlu.cai@zmaw.de

DOI: 10.1175/JCLI-D-13-00674.1

© 2014 American Meteorological Society

a functional relationship between water demand by net radiation (or potential evapotranspiration) and water supply by precipitation. It reduces the complex mutual interactions between climate and hydrological processes to a single parameter, the dryness as the ratio of two fluxes: mean annual net radiation versus precipitation. These two fluxes represent the forcing components of the surface energy and water flux balances closely linked to productivity and distribution of vegetation controlling its state, growth, and decay (Donohue et al. 2009; Fraedrich and Sielmann 2011; Potter et al. 2005; Williams et al. 2012; for a theoretical analysis, see Fraedrich 2010).

Two aspects of the climate–vegetation combination are commonly separated describing the effects of (i) climate on vegetation and (ii) vegetation on climate. They are related to the rainfall–runoff chain partitioning rainfall into runoff and evaporation. In addition (see, e.g., Voepel et al. 2011) climate control of the rainfall–runoff chain is considered to be of first order occurring on the conditions of spatial scale $>10\,000\,\mathrm{km}^2$ and temporal scale $\gg 1\,\mathrm{yr}$ (Donohue et al. 2007). On the other hand, control by vegetation dynamics, which includes the dependence on soil and seasonality (associated with scales $< 1000\,\mathrm{km}^2$), is considered to be of second order (Zhang et al. 2001). That is, in the Budyko framework, catchments are assumed to be at steady state and driven by the macroclimate so that the hydrological role of vegetation dynamics does not need to be explicitly considered for applications on large spatial and temporal scale. On the other hand, analyzing the role of vegetation for climate and water ranging from long term to interannual and seasonal scales (Wang and Alimohammadi 2012; Zanardo et al. 2012; Zhang et al. 2004; and many others), vegetation was found to be more dependent on the Horton index compared to Budyko's dryness index (e.g., Troch et al. 2009; Voepel et al. 2011).

Our analysis is gridcell based with a resolution of 0.75° ($\ll 10\,000\,\mathrm{km}^2$) to provide global statistics. Besides that, remote sensing–based time series show potential in incorporating measures of vegetation dynamics into the Budyko framework, which, to our knowledge, is a relatively new field of research. By incorporating such measures, it may be possible to extend the Budyko framework of analysis (Li et al. 2013; Yang et al. 2009; Zhang et al. 2001) to applications on small scales. Such a modified Budyko framework is expected to predict the hydrological effects of vegetation management activities and to explore the possible implications of short and long-term climate change on both vegetation and hydrology.

To our knowledge, only Azzali and Menenti (2000) have analyzed the relation between different magnitudes of long-term mean aridity with vegetation types and their foliar phenology in South Africa. Here we extend this analysis globally. After introducing ERA-Interim and NVDI remote sensing data (section 2), the Budyko framework of geobotanic climate diagnostics is presented, comparing climate dryness and vegetation greenness (section 3). Means and variability are analyzed (section 4), followed by a concluding summary.

2. Data, methods of analysis, and geographical setting

Both the ERA-Interim and GIMMS datasets (25-yr averages: 1982–2006; see Balsamo et al. 2012; Tucker et al. 2005) are projected within geographic latitude/longitude. For combination and better interpretation, NDVI annual, summer (June–August), and winter means (December–February) are calculated. The spatial resolutions of the ERA-Interim and GIMMS datasets are $0.75° \times 0.75°$ and $8\,\mathrm{km} \times 8\,\mathrm{km}$, respectively. To be comparable, we resample the relatively higher-resolution GIMMS NDVI dataset into $0.75° \times 0.75°$ by bilinear resampling. The final size of global maps in this study is represented by 480×184 pixels (without poles).

The climatological setting (1982–2006) is displayed in terms of geographical distributions (Fig. 1) as follows:

(i) The climate mean dryness ratio (mean energy to mean water supply; Budyko 1974), which provides a climatological measure of vegetation, is obtained from the ERA-Interim mean net radiative and water fluxes, N and P. The dryness ratio, $D = N/P$, quantifies the climate's water (or energy) limitation separated at $D = 1$. According to Budyko (1974), we divide the dryness into five ranges (Fig. 1a). To complement the geographical distribution of the dryness ratio D, the total energy–water supply $N + P$ is displayed in Fig. 1c (interval = $1\,\mathrm{m\,yr}^{-1}$). Note that ERA-Interim energy fluxes are provided as half-day integrals [$\mathrm{J\,m}^{-2}\ (12\,\mathrm{h})^{-1}$ or $2(365)\,\mathrm{J\,m}^{-2}\,\mathrm{yr}^{-1}$] and converted to water equivalents of $10^3\,\mathrm{kg\,m}^{-2}\,\mathrm{yr}^{-1}$ (or $\mathrm{m\,yr}^{-1}$) using the latent heat for condensation of water, $L = 0.25 \times 10^7\,\mathrm{J\,kg}^{-1}$ at 0°C. Thus, an energy flux of $1\,\mathrm{J\,m}^{-2}\,(12\,\mathrm{h})^{-1}$ yields a water flux equivalent of $2.920 \times 10^{-7}\,\mathrm{m\,yr}^{-1}$.

(ii) Vegetation is presented by NDVI: Very low values (<0.1) correspond to barren areas, sand, or snow. Low values represent shrub and grassland (0.2–0.3), followed by a moderate transition range (0.3–0.6) and high values characterizing temperate and tropical rain forests (0.6–0.8) (Weier and Herring 2005; Wittich and Hansing 1995). Accordingly, we divide NDVI into three ranges (Fig. 1b): low (0.1–0.3), moderate (0.3–0.6), and high (0.6–0.8 and larger).

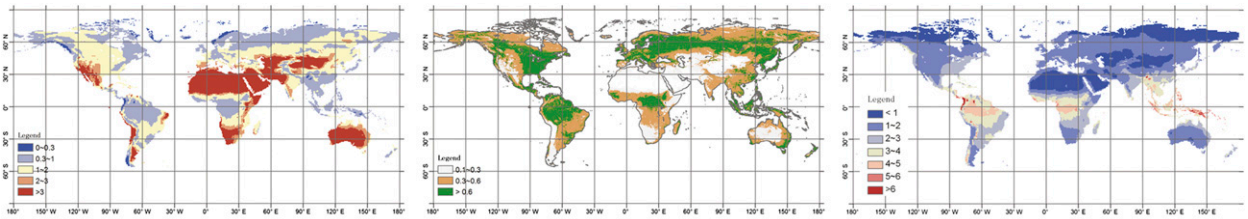

FIG. 1. Geographical distribution of climate means (1982–2006): (a) dryness ratio of net radiation and rainfall $D = N/P$ (from ERA-Interim), (b) the satellite-based NDVI greenness vegetation index from remote sensing data [very low values of NDVI (0.1 and below) correspond to barren areas, sand, or snow; moderate values represent shrub and grassland (0.2–0.3); and high values indicate temperate and tropical rain forests (0.6–0.8)], and (c) the total supply of energy and water $N + P$ (calculated from ERA-Interim).

3. A surface climate state space

The rainfall–runoff chain receives a total supply of energy and water that is net radiation N and rainfall P, which is $N + P$. These processes are measured in terms of flux densities, which satisfy the respective long-term mean balance equations at the earth's surface. That is, water is supplied by precipitation P and balanced by streamflow or runoff Ro plus evapotranspiration E. Energy is supplied by net radiation N and balanced by sensible plus latent heat fluxes H and E (energy flux units in water flux equivalents; m yr^{-1}),

$$P = \mathrm{Ro} + E \quad \text{and}$$

$$N = H + E.$$

As in hydrodynamical flows, flux ratios provide useful parameters to span the system's state space, to locate states and to identify processes underlying the rainfall–runoff chain. One parameter is the flux ratio of energy and water supply, that is of net radiation and rainfall, which has been introduced by Budyko (1974) as dryness (or its inverse, as wetness),

$$D = N/P,$$

separating energy-limited regimes ($D < 1$ or $N < P$) from water-limited ones ($D > 1$, $N > P$) at $D = 1$.

a. (N, D) diagram

In Budyko's framework climate states can embedded in a two-dimensional state space (Fig. 2a). Spanned by net radiation N (representing meridionality; see Fig. 1) and dryness D this diagram spans the climate mean sources of the rainfall–runoff chain providing the input to the water and energy budget.

(i) The state space displays climate variables such as precipitation, presented by the slopes of isolines through the origin, $N = PD$, and the isolines of total supply, $N = (P + N)[D/(D + 1)]$, attain the slope of $N + P$ at the origin ($N = D = 0$).

(ii) The state space has also been used to include the biosphere into a physical-based framework of climate analysis. Interpreting the energy input N as potential evapotranspiration the dryness or aridity index represents the flux ratio of water demand to supply. Budyko (1974) has introduced quantitative geobotanically relevant thresholds for land surface climate states, which relate dryness to vegetation structures (Fig. 2b): Tundra, $D < 1/3$, and forests, $1/3 < D < 1$, are energy limited ($D < 1$), because available energy N is low, so that runoff exceeds evaporation for given precipitation, $E \sim N$. Steppe and savanna, $1 < D < 2.0$; semidesert, $2.0 < D < 3.0$; and desert, $3.0 < D$, are water-limited climates ($D > 1$), where the available energy is so high that water supplied by precipitation evaporates, which then exceeds runoff, $E - P$.

b. Climatological setting in state space: Frequency distribution of ERA-Interim surface climate states

The probabilistic measure of the equilibrium surface climate in state space comprising the results of the common global geographical distributions of net radiation and dryness in terms of frequencies of net radiation–dryness (N, D) pairs to represent meridionality and zonality in Budyko's framework. The physical states in the (N, D) diagram are characterized by the number density of area units of (N, D) pairs, whose long-term means (1982–2006) are obtained from the ERA-Interim dataset (Fig. 2c) as follows:

(i) The boundary (full line) includes all 26 692 continental pixels (with $N > 0$) associated with (N, D) pairs on the global land surface. The zero frequency boundary (or contour line) is comparable with Budyko (1974, see Fig. 2b).

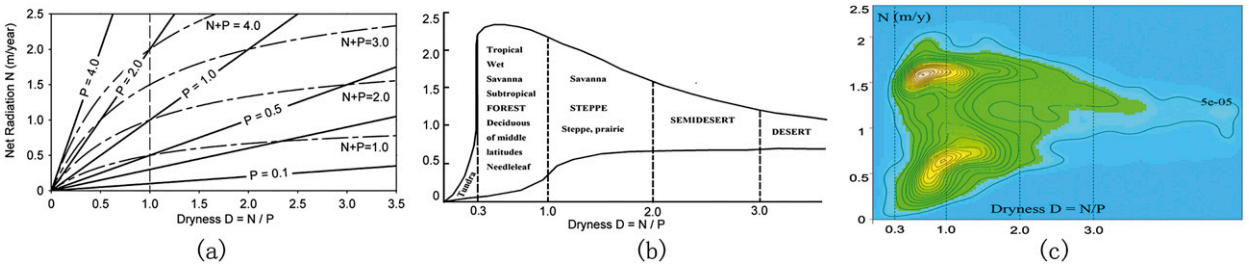

FIG. 2. Continental surface climate state space or (N, D) diagram spanned by the mean net radiation N and dryness ratio D (all units in m yr^{-1} water equivalent). (a) Precipitation $N = PD$ corresponds to the slope of straight lines through the origin; the curve of total supply of energy and water satisfies $N = (N + P)[D/(D + 1)]$. (b) Geobotanic zonality types are adapted from Budyko (1974, Fig. 103); the boundary (full line) includes all area units of (N, D) pairs observed on the global land surface; and D classes are separated by vertical lines (dashed) with additional subclasses depending on the magnitude of net radiation. (c) Frequency distribution of the climatological means of net radiation and dryness or (N, D) pairs (from ERA-Interim); the total land area corresponds to the total number of equal area units. The $D = 1$ threshold separating energy-limited from water-limited regimes (vertical line) is included.

(ii) The global frequency distribution in the (N, D) diagram is characterized by two modes separated by meridional differentiation (net radiation), while the distribution of dryness is unimodal with its maximum close to the separation of energy- and water-limited regimes. The modes can be associated with Budyko's geobotanic classes (Fig. 2b) related to Northern and Southern Hemisphere climates. Separating the global data into the Northern and Southern Hemisphere (not shown), each one contributes a peak: (a) The Northern Hemisphere is predominantly occupied with deciduous needle leaf forest (energy-limited domain) and then followed by the steppe–prairie type thereby crossing the threshold from energy to water-limited regime (lower peak). (b) The Southern Hemisphere is mainly characterized by tropical forest and wet savanna in the energy-limited regime followed by savanna-type vegetation when crossing the same border (upper peak). (c) We note that two modes of frequent (N, D) pairs characterize statistically preferred climate states which, in the (N, D) diagram, straddle the ($D = 1$) threshold.

(iii) The "ridges" of the probability density function appear to follow the curves of constant total energy and water supply with a correlation coefficient of $r \sim 0.49$ for the lower ridge near $(N + P) \sim 1$–$2\,\mathrm{m\,yr^{-1}}$ and $r \sim 0.1$ for the upper ridge $(N + P) \sim 1$–$2\,\mathrm{m\,yr^{-1}}$, respectively (see Fig. 2a). Although significant, only the lower ridge (dominated by the midlatitude climates near $D \sim 1 \pm 0.2$; see section 3b) shows sufficiently high correlation to support the hypothesis that a majority of climate pixels satisfy the constant total energy supply governing the structure of the frequency distribution density. The interpretation in terms of atmospheric dynamics requires further analysis.

4. Vegetation in the climate state space: Means and variability

For a comparison with Budyko's dryness–vegetation relation we include greenness information (GIMMS NDVI data) into the ERA-Interim (1982–2008) surface climate or (N, D) state space. These (N, D) pairs are combined to (N, D, NDVI) triplets, which are presented as scatterplots (Figs. 3a–c): High values [Fig. 3a: NDVI > 0.75 (dark green) and 0.75 > NDVI > 0.6 (light green)] characterize temperate and tropical rain forests (0.6–0.8) (Weier and Herring 2013; Wittich and Hansing 1995) straddling $D = 1$.

Some green pixels in the net radiation domain of tropical latitudes extend far into the high dryness regime, which can be associated with mangroves. Projecting forest pixels with $D \sim 2$–3, into the geographic space reveal only a small area with net radiation $N > 2\,\mathrm{m\,yr^{-1}}$ (box inserted in Fig. 3a). This vegetation (denoted as forests) prevails along coastal regions, which explains the external water supply provided by seawater, and also the forest type to be mangrove (Fig. 3b; Spalding et al. 2013). Compared to the high greenness concentration, the low values corresponding to barren areas, sand, shrub, and snow are widely distributed in the (N, D) diagram (Fig. 3d), in regions of higher dryness. Note that moderate NDVI ranges also share surface climate states with high NDVI greenness (Fig. 3c).

a. Climate mean

The scatterplots are further analyzed in terms of smoothed frequency diagrams (Fig. 4) presenting the climate mean states as long-term (1982–2006) mean (N, D, NDVI) triplets for the Northern and Southern Hemisphere, and for Northern Hemisphere summer and winter seasons.

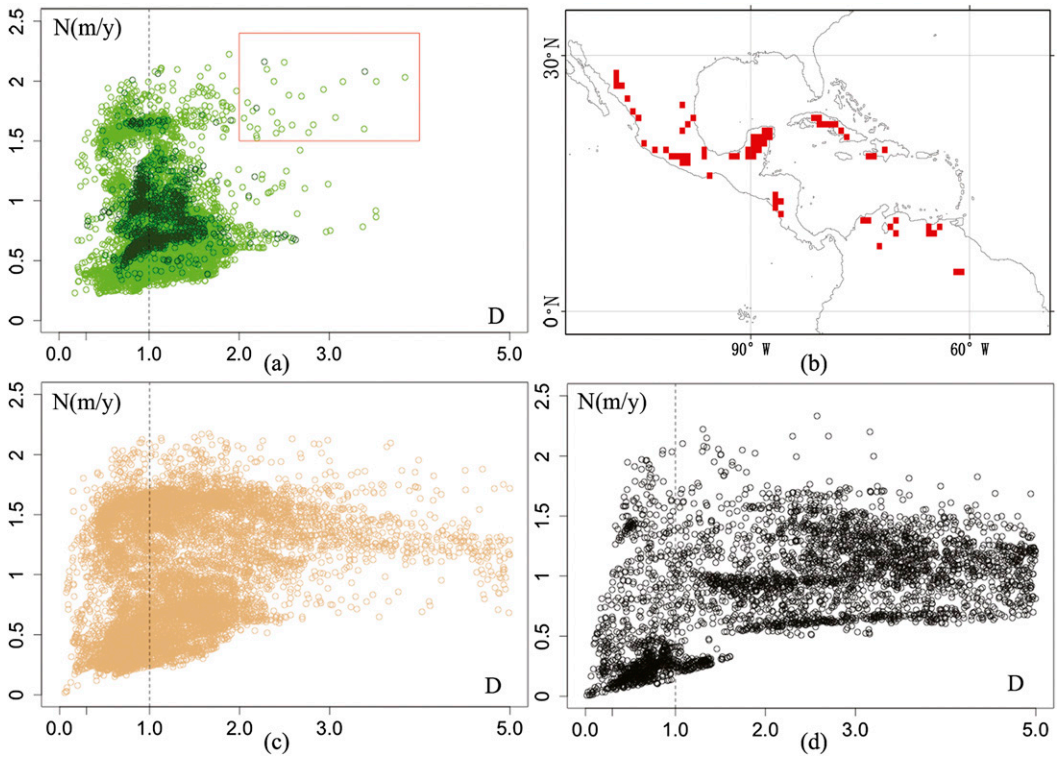

FIG. 3. Northern Hemisphere NDVI greenness vegetation scatterplot in the net radiation dryness (N, D) diagram of Earth's surface climate (units in m yr^{-1} water equivalent): (a) high values with NDVI > 0.6 (dark green: NDVI > 0.75; light green: 0.75 > NDVI > 0.6), where the inserted rectangular frame denotes mangrove pixels, whose (b) geographic locations are also presented; (c) medium values with 0.6 > NDVI > 0.3; and (d) small values with 0.3 > NDVI > 0.1.

(i) Forests exist predominantly in the dryness range from 0.3 to 1.5 straddling the $D = 1$ threshold, and sparse vegetation regions appear in $D > 3$. The similarities are more pronounced in the distributions of Northern Hemisphere annual and summer means. Separating Northern Hemisphere summer and winter reduces the, frequency of occurrence of high NDVI values (forests attributed to the midlatitudes).

(ii) Vegetation in midlatitudes captured by satellite can be influenced by climate variables, such as snow cover. That is, the NDVI summer means in the Northern Hemisphere are considered to be a more realistic climatological measure of vegetation compared to the annual and winter means. The satellite-based Northern Hemisphere summer vegetation distribution, however, is still shifted to dryness $D > 1$.

(iii) For large net radiation ($N \sim 2\,\mathrm{m\,yr^{-1}}$), forests extend to $D \sim 2$–3, where evaporation (in ERA-Interim and several climate models) exceeds precipitation and hence runoff ($P - E$) is negative. That is, external water supply is required for these regions, such as rivers terminating for land irrigation, supplying closed watersheds or lakes. However, for proving the latter to be actually observed, further analyses on accurate estimates of evapotranspiration are required.

(iv) Satellite-based Northern Hemisphere summer and winter mean (Figs. 4c,d) separate deciduous midlatitude needle leaf forests from tropical to subtropical forests (Budyko 1974; Fig. 2), because deciduous forests do not show greenness in winter. Thus, subtracting the winter from the summer mean distribution (not shown) reveals deciduous midlatitude needle leaf forests.

b. *Interannual variability*

The combination of ERA-Interim climate and GIMMS NDVI vegetation information in the (N, D) diagram provides a suitable background to extend the analysis beyond the first moments and to include interannual variability. The coefficient of variation as the ratio of standard deviation to the mean (or inverse of signal to noise ratio) is used to compare the measure of dryness (ERA-Interim) and NDVI (Fig. 5). A small coefficient

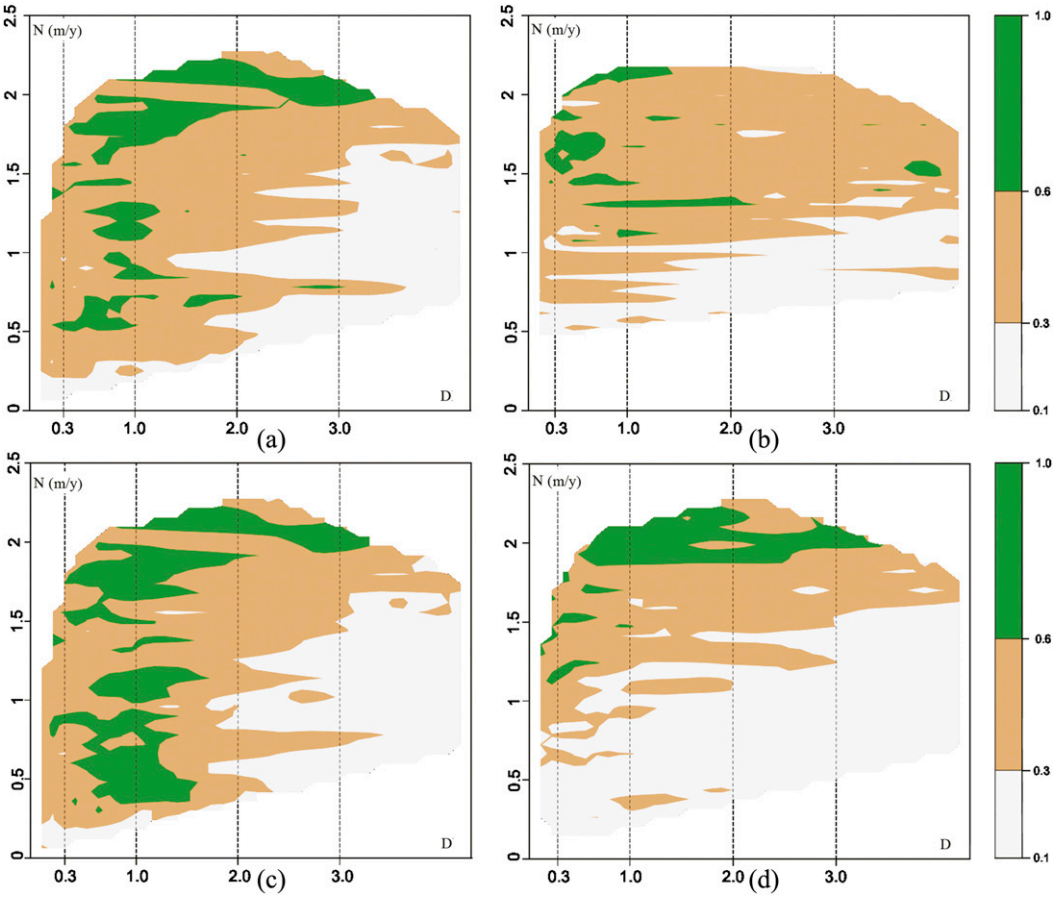

FIG. 4. NDVI vegetation in the net radiation dryness (N, D) diagram (units in m yr^{-1} water equivalent; smoothing by linear interpolation): (a) Northern Hemisphere, (b) Southern Hemisphere, and Northern Hemisphere (c) summer and (d) winter.

of dryness variation demonstrates that high values of climate mean NDVI (straddling $D = 1$; see Figs. 3a, 4a,b) favor regions with small dryness variability or, vice versa, the green vegetation (associated with forests) leads to small variations of dryness (Fig. 5a). Figure 5b demonstrates this showing that the median of the coefficients of variation binned in NDVI classes of greenness (width of 0.1) clearly decrease with increasing dryness. Apparently vegetation greenness tends to smooth the volatility of the year-to-year fluctuations of dryness. That is, large NDVI greenness of vegetation straddles the water–energy limitation (at $D = 1$) where also minimum values of the coefficient of year-to-year dryness variation are attained. The dryness variation versus dryness mean boxplot (Fig. 5c) supports the analysis. Note that bins in Fig. 5c are chosen according to Budyko's D classification (Fig. 2b) for $D < 1$; for $1 < D < 3$ Budyko's $D = 0.5$ intervals are used (to demonstrate details of D variability near the $D = 1$ water–energy-limited regimes). Values for desert conditions are grouped in a single class, $D > 3$. A change of the binning (in $D = 0.5$ and $D = 0.25$ intervals) did not change the results (not shown).

5. Conclusions

Statistics and structures of remote sensing information on vegetation are commonly analyzed in terms of geographical distributions. To supplement these analyses we embed the information in Budyko's two-dimensional state space spanned by physically relevant surface climate variables: Net radiation N, interpreted as potential evapotranspiration, represents the source term of the energy balance equation, characterizes meridional differentiation, and provides a measure of water demand; the dryness ratio D (water demand versus supply) includes rainfall as source of the water budget. In geographic space, vegetation (NDVI pixels) is associated with the earth's surface climate variables (ERA-Interim data) leading to (N, D, NDVI) triplets. Analysis of the 25-yr high-resolution ERA-Interim and NDVI data

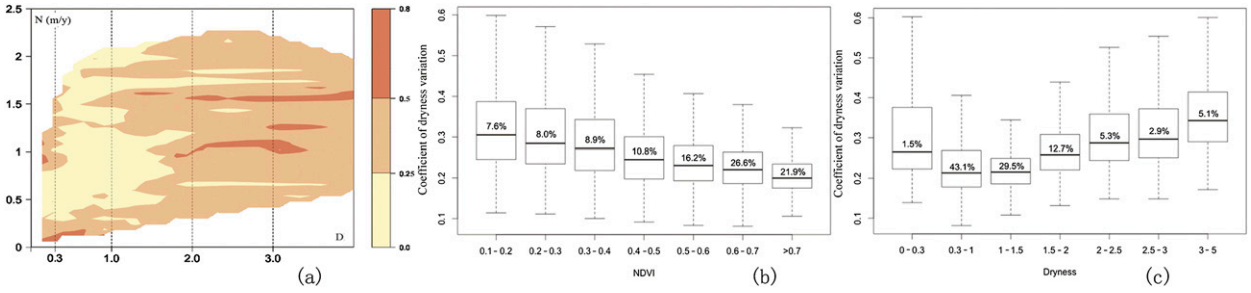

FIG. 5. (a) Coefficient of year-to-year dryness variation (ratio of standard deviation to climate mean): (a) in (N, D) state space (smoothing by linear interpolation). Box plots present the statistics of the coefficients of dryness variation depending on (b) mean NDVI greenness vegetation and (c) mean dryness D.

on a gridpoint-to-gridpoint basis yields the following results:

(i) The ERA-Interim surface climate embedded in the net radiation and dryness (N, D) diagram shows a bimodal frequency distribution of unit areas concentrated in the energy-limited climate regime (with dryness $D < 1$) but separated meridionally with higher and lower net radiation. Considering only the Southern (Northern) Hemisphere, a single mode of high (reduced) water demand prevails in the humid tropics (midlatitudes).

(ii) The extended state space of climate mean (N, D, NDVI) triplets connects the global distribution of unit areas attached to the physical ERA-Interim and the NDVI dataset. Meridionality and dryness demonstrate that high NDVI values (temperate and tropical forests; 0.6–0.8) occupy both energy- and water-limited regimes straddling the $N \sim P$ demarcation line: that is, forests are not restricted to the energy-limited domain $D < 1$ as in Budyko's (1974) geobotanic classification (see Fig. 2b). Extensions deep into the water-limited regime represent marginal coastal habitats of mangroves sustained by external water supply.

(iii) Combining the (N, D, NDVI) analysis of climate means with interannual dryness variability shows that tropical and temperate forests (NDVI > 0.6) are associated with low interannual dryness variability. That is, in the long-term mean the coefficient of interannual dryness variation decreases with increasing NDVI (vegetation greenness) and therefore attains a minimum which also straddles the threshold ($D = 1$) separating water- and energy-limited regimes.

Surface climate analysis in Budyko's geobotanic state space provides a suitable process-based physical framework to analyze the vegetation–climate relation, including measures of interannual variability. Thus, analyzing links between changes of vegetation and climate does not only require considerations of the impact of changing climate means (of rainfall and radiation) but also changes of their respective interannual variability.

Acknowledgments. Support by the Chinese Science Database (XXH12504-1-12, as a participator) and the Joint CAS-MPG PhD-Program (DC) and the Max Planck Fellow Group (DC and KF) and the hospitality of the KlimaCampus, University of Hamburg, are acknowledged. Thanks for the constructive reviewers' comments.

REFERENCES

Asrar, G., M. Fuchs, E. Kanemasu, and J. Hatfield, 1984: Estimating absorbed photosynthetic radiation and leaf area index from spectral reflectance in wheat. *Agron. J.,* **76,** 300–306, doi:10.2134/agronj1984.00021962007600020029x.

Azzali, S., and M. Menenti, 2000: Mapping vegetation-soil-climate complexes in southern Africa using temporal Fourier analysis of NOAA-AVHRR NDVI data. *Int. J. Remote Sens.,* **21,** 973–996, doi:10.1080/014311600210380.

Balsamo, G., and Coauthors, 2012: A global land-surface reanalysis based on ERA-Interim meteorological forcing. ERA Rep. 13, 25 pp.

Budyko, M., 1956: *The Heat Balance of the Earth's Surface.* U.S. Weather Bureau, 259 pp.

——, 1974: *Climate and Life.* Vol. 18, Academic Press, 508 pp.

——, S. Lemeshko, and V. Yanuta, 1986: *The Evolution of the Biosphere.* D. Reidel, 423 pp.

Carlson, T. N., and D. A. Ripley, 1997: On the relation between NDVI, fractional vegetation cover, and leaf area index. *Remote Sens. Environ.,* **62,** 241–252, doi:10.1016/S0034-4257(97)00104-1.

Donohue, R. J., M. L. Roderick, and T. R. McVicar, 2007: On the importance of including vegetation dynamics in Budyko's hydrological model. *Hydrol. Earth Syst. Sci. Discuss.,* **11,** 983–995, doi:10.5194/hess-11-983-2007.

——, T. R. McVicar, and M. L. Roderick, 2009: Climate-related trends in Australian vegetation cover as inferred from satellite observations, 1981-2006. *Global Change Biol.,* **15,** 1025–1039, doi:10.1111/j.1365-2486.2008.01746.x.

Fraedrich, K., 2010: A parsimonious stochastic water reservoir: Schreiber's 1904 equation. *J. Hydrometeor.,* **11,** 575–578, doi:10.1175/2009JHM1179.1.

——, and F. Sielmann, 2011: An equation of state for land surface climates. *Int. J. Bifurcation Chaos,* **21,** 3577–3587, doi:10.1142/S021812741103074X.

Köppen, W., 1936: *Das Geographische System der Klimate.* Handbuch der Klimatologie, Borntraeger, 46 pp.

Li, D., M. Pan, Z. Cong, L. Zhang, and E. Wood, 2013: Vegetation control on water and energy balance within the Budyko framework. *Water Resour. Res.,* **49,** 969–976, doi:10.1002/wrcr.20107.

Myneni, R. B., F. G. Hall, P. J. Sellers, and A. L. Marshak, 1995: The interpretation of spectral vegetation indexes. *IEEE Trans. Geosci. Remote Sens.,* **33,** 481–486, doi:10.1109/36.377948.

Potter, N., L. Zhang, P. Milly, T. McMahon, and A. Jakeman, 2005: Effects of rainfall seasonality and soil moisture capacity on mean annual water balance for Australian catchments. *Water Resour. Res.,* **41,** W06007, doi:10.1029/2004WR003697.

Spalding, M. D., F. Blasco, and C. D. Field, cited 2013: Global distribution of mangroves (version 3). UNEP World Conservation Monitoring Centre and International Society for Mangrove Ecosystems dataset. [Available online at http://data.unep-wcmc.org/datasets/6.]

Troch, P. A., and Coauthors, 2009: Climate and vegetation water use efficiency at catchment scales. *Hydrol. Processes,* **23,** 2409–2414, doi:10.1002/hyp.7358.

Tucker, C. J., J. Pinzon, and M. Brown, 2004: Global inventory modeling and mapping studies. University of Maryland Global Land Cover Facility Rep. NA94apr15b(11), 20 pp.

——, ——, ——, D. A. Slayback, E. W. Pak, R. Mahoney, E. F. Vermote, and N. El Saleous, 2005: An extended AVHRR 8-km NDVI dataset compatible with MODIS and SPOT vegetation NDVI data. *Int. J. Remote Sens.,* **26,** 4485–4498, doi:10.1080/01431160500168686.

Voepel, H., B. Ruddell, R. Schumer, P. A. Troch, P. D. Brooks, A. Neal, M. Durcik, and M. Sivapalan, 2011: Quantifying the role of climate and landscape characteristics on hydrologic partitioning and vegetation response. *Water Resour. Res.,* **47,** W00J09, doi:10.1029/2010WR009944.

Wang, D., and N. Alimohammadi, 2012: Responses of annual runoff, evaporation, and storage change to climate variability at the watershed scale. *Water Resour. Res.,* **48,** W05546, doi:10.1029/2011WR011444.

Weier, J., and D. Herring, cited 2013: Measuring vegetation (NDVI and EVI). NASA Earth Observatory Library. [Available online at http://earthobservatory.nasa.gov/Features/MeasuringVegetation/.]

Williams, C. A., and Coauthors, 2012: Climate and vegetation controls on the surface water balance: Synthesis of evapotranspiration measured across a global network of flux towers. *Water Resour. Res.,* **48,** W06523, doi:10.1029/2011WR011586.

Wittich, K., and O. Hansing, 1995: Area-averaged vegetative cover fraction estimated from satellite data. *Int. J. Biometeor.,* **38,** 209–215, doi:10.1007/BF01245391.

Yang, D., W. Shao, P. J.-F. Yeh, H. Yang, S. Kanae, and T. Oki, 2009: Impact of vegetation coverage on regional water balance in the nonhumid regions of China. *Water Resour. Res.,* **45,** W00A14, doi:10.1029/2008WR006948.

Zanardo, S., C. J. Harman, P. A. Troch, P. S. C. Rao, and M. Sivapalan, 2012: Intra-annual rainfall variability control on interannual variability of catchment water balance: A stochastic analysis. *Water Resour. Res.,* **48,** W00J16, doi:10.1029/2010WR009869.

Zhang, L., W. Dawes, and G. Walker, 2001: Response of mean annual evapotranspiration to vegetation changes at catchment scale. *Water Resour. Res.,* **37,** 701–708, doi:10.1029/2000WR900325.

——, K. Hickel, W. R. Dawes, F. H. S. Chiew, A. W. Western, and P. R. Briggs, 2004: A rational function approach for estimating mean annual evapotranspiration. *Water Resour. Res.,* **40,** W02502, doi:10.1029/2003WR002710.